Complex Principal Oscillation Pattern Analysis

GERD BÜRGER

Max-Planck-Institut für Meterologie, Hamburg, Germany

(Manuscript received 1 June 1992, in final form 18 March 1993)

ABSTRACT

Complex principal oscillation pattern (CPOP) analysis is introduced as an extension of conventional POP analysis. Both are intended to resolve regular evolving patterns from processes with many degrees of freedom. While POP analysis, like many other techniques, deals with the concept of the *system state* as a real vector, it is argued that this notion be extended into the complex domain. The approach used here results from a critical review of the theory of linear systems of first order. It turns out that these systems cannot appropriately model standing oscillations. The notion of the traveling rate of a mode is defined, and it is demonstrated that the mode's frequency and traveling rate are directly coupled via the system matrix. One consequence is that clean standing oscillations cannot be modeled by linear systems of first order.

CPOP analysis introduces a new vector of state. By defining the complex state "state + $i \cdot$ momentum," both the conventional state itself and its momentum are simultaneously described. The method is capable of resolving oscillatory patterns of any given traveling rate from a stationary process. First experiments show that the CPOPs evolve more regularly and with less noise than corresponding POPs. A prediction scheme that is appropriate for CPOPs is defined by introducing a transformation technique that can be considered as a *causal Hilbert transform*. With this scheme prediction skills that are significantly stronger than those of the POP model are gained.

1. Introduction

A characteristic problem in climatological studies is that the involved processes are usually of very high complexity with a huge number of degrees of freedom. Although each of these free components might, at a certain time, play a crucial role, there is a general consensus that many important features of the climate system are governed by rather low-order dynamical subsystems. If this is true, one can decompose the state of the system into a deterministic and a random portion. The major task for the climate statistician is, therefore, to find the right decomposition or, at least, to extract significant physical signals from the noisy system.

There are several methods to reduce complex processes to lower-order ones, such as: empirical orthogonal functions (EOFs) and their complex form (CEOFs), singular value decomposition (SVD), canonical correlation analysis (CCA), and principal interaction and oscillation patterns (PIPs and POPs). Common to all methods is that they normally reduce the number of degrees of freedom by at least one order of magnitude. This is achieved by splitting the space–time variability of the process in question into the time-variability of some generic spatial patterns.

Corresponding author address: Dr. Gerd Bürger, Lamont-Doherty Geophysical Observatory, Columbia University, Route 9W, Palisades, NY 10964.

Each has its own advantages and disadvantages. For instance, EOFs are a very elegant and simple tool to derive statistically and geometrically orthogonal patterns. With some particular exceptions (see North 1984) this approach is generally nondynamical, and so the physical interpretation of the patterns often remains an unsolved question. POP analysis is, by definition, a dynamical approach, but the POP patterns normally lack orthogonality. Hasselmann (1988) argues that with respect to space–time variability the POP technique appears superior to many other techniques since it extracts dominant features at dominant frequencies. For example, for prescribed frequency bands, the POPs should reduce to CEOFs.

In this paper we introduce complex principal oscillation pattern (CPOP) analysis. POPs are not in every case superior to EOFs. As an example, we demonstrate that POP analysis is *unable to resolve standing oscillations*, a capability shared by all EOF techniques. Moreover, we show that the impossibility of modeling standing oscillations is inherent in any linear system of first order. In a certain sense, CPOP analysis emerges from POP analysis just as the CEOFs emerge from EOFs. While the CEOF analysis is able to resolve traveling features, which are invisible for the EOF technique, the CPOPs now comprise standing features, which cannot be found by POPs.

The main lines of the CPOP model are very similar to those of the POP model. Therefore, as far as both models coincide we will not go into the details. They

are best described in Storch et al. (1988). The dynamical aspects of both models can be summarized in the following manner.

It is at the heart of all the statistical techniques that, given a process of high complexity, it is possible to decompose the process into a deterministic part and a random part. The idea presented by Hasselmann (1988) is that once we know the general structure of the physical laws that govern the deterministic part, we can *estimate* the actual parameters of these laws *from the data,* together with the projection patterns. This is the general PIP concept.

In the POP approach we predetermine the physical system to be *linear.* This can be justified empirically by the fact that many of the climatic features indeed arise from waves and oscillations. Theoretically one can argue that as long as there exists a *basic state* of the system, the perturbations about this basic state will be governed by linear dynamics, just as in classical perturbation theory. The POPs describe the modes of this linear system. We will sketch the main issues of the POP model in sections 2 and 3.

In section 4 we introduce the *traveling rate* of a mode and show that, for a given linear system of first order, the frequency of the mode is bounded only by the norm of the system matrix and this traveling rate, yielding the impossibility of modeling standing oscillations.

In section 5 we show that to adequately model an oscillation one must have, for each oscillating component of the system, a further *conjugate component,* which oscillates in the same way but with a different phase (shifted by $\pi/2$). In Hamiltonian mechanics this is taken into account by considering a priori the $2n$-dimensional phase space of *state and momentum,* with n being the degree of freedom of the system. In this formulation a standing oscillation of the state is turned into a cycle of state and momentum.

In our approach toward pattern analysis we follow the same lines: we model state and momentum simultaneously. But unlike Hamiltonian mechanics, we do not work in a $2n$-dimensional real phase space but in an n-dimensional *complex phase space.* That means we consider the *complex vector of state* "state $+ i \cdot$ momentum," where momentum is defined by means of the Hilbert transform. Rewriting the POP formalism in this new complex setting leads to the CPOP analysis, which is introduced in detail in section 6.

The seventh section is devoted to testing the CPOP model with three sorts of data:

1) a series of synthetical low-order processes with known modes;
2) monthly mean sea surface temperatures containing the El Niño mode;
3) daily tropical winds containing the Madden–Julian Oscillation.

The last section contains the CPOP prediction scheme. Many aspects of this scheme, like the causal Hilbert transform, are still under some development. Nevertheless, our results indicate that even in this rough state the CPOP prediction achieves higher skill than the POP prediction. We do not include any comparison to other techniques.

2. The modes of a linear system

This and the next section provide a short introduction to the POP model. For details we refer the reader to Hasselmann (1988) and Storch et al. (1988). A (discrete) linear system $\mathcal{S}$ of dimension n is given by an evolution equation:

$$\mathbf{q}(t+1) = \mathcal{A}\mathbf{q}(t), \tag{1}$$

where $\mathbf{q}(t)$ denotes the n-dimensional state vector of $\mathcal{S}$ at time t, and $\mathcal{A}$ is the n-dimensional system matrix of $\mathcal{S}$. (As only one time step is modeled, we say that $\mathcal{S}$ is of *first order.*) This is a set of n coupled linear equations. They are usually solved by expanding $\mathbf{q}$ in terms of the n complex eigenvectors $\mathbf{M}_1, \ldots, \mathbf{M}_n$ of $\mathcal{A}$,

$$q(t) = \gamma_1(t)\mathbf{M}_1 + \cdots + \gamma_n(t)\mathbf{M}_n. \tag{2}$$

The eigenvectors $\mathbf{M}_j$ are known as the *modes of* $\mathcal{S}$. Inserting (2) into (1) yields a set of n uncoupled evolution equations for the complex coefficients γ_j,

$$\gamma_j(t+1) = \lambda_j\gamma_j(t), \tag{3}$$

where λ_j is the jth eigenvalue of $\mathcal{A}$. The solution of (3) is straightforward:

$$\gamma_j(t) = \lambda_j^t. \tag{4a}$$

Utilizing the polar representation for $\lambda_j = \lambda = \rho \cdot e^{i\omega}$, (we omit the index j) this can be written as

$$\gamma(t) = \rho^t e^{i\omega t}. \tag{4b}$$

Hence, the complex mode coefficient evolves as a damped spiral in the complex plane, with a characteristic damping rate ρ and frequency ω. As we will see below, these two numbers play a crucial role for both POP and CPOP analysis since they mainly characterize the "quality" of the analyzed patterns. Physically, this has a very simple meaning; denoting the real and imaginary part of a complex quantity by the superscripts $^{\mathrm{R}}$ and $^{\mathrm{I}}$, respectively, we can write the mode $\mathbf{M}$ as $\mathbf{M} = \mathbf{M}^{\mathrm{R}} + i \cdot \mathbf{M}^{\mathrm{I}}$. The evolution $m(t) = \gamma(t) \cdot \mathbf{M}$ of the mode $\mathbf{M} = \mathbf{m}(0)$ can thus be written:

$$\mathbf{m}^{\mathrm{R}}(t) = \rho^t[\cos(\omega t)\mathbf{M}^{\mathrm{R}} - \sin(\omega t)\mathbf{M}^{\mathrm{I}}] \tag{5R}$$

$$\mathbf{m}^{\mathrm{I}}(t) = \rho^t[\cos(\omega t)\mathbf{M}^{\mathrm{I}} + \sin(\omega t)\mathbf{M}^{\mathrm{R}}]. \tag{5I}$$

Note that $\mathbf{m}^{\mathrm{I}}(t) = \mathbf{m}^{\mathrm{R}}(t - P/4)$, with the period $P = 2\pi/\omega$.

For a real system matrix $\mathcal{A}$ the modes occur in complex conjugate pairs (if they are complex at all). Two such complex conjugate modes represent the same real process $\mathbf{m}^{\mathrm{R}}(t)$. The full real-mode signal is then given

by $2\mathbf{m}^R(t)$, whereas the two imaginary parts $\mathbf{m}^I(t)$ cancel. Thus the general evolution of a damped mode ($\rho \leqslant 1$) can be described in a two-dimensional subspace spanned by the patterns $\mathbf{M}^R$ and $\mathbf{M}^I$, as in a succession of

$$\mathbf{M}^I \rightarrow \mathbf{M}^R \rightarrow -\mathbf{M}^I \rightarrow -\mathbf{M}^R \rightarrow \mathbf{M}^I. \quad (6)$$

The general solution of (1), that is, each possible time evolution $q(t)$ of the system $\mathcal{S}$, is a superposition of n single-mode evolutions of the above kind. In this way the modes describe the system $\mathcal{S}$ completely.

3. Estimating the modes: POPs

In section 2 we discussed the output of a linear system as a function of system parameters. In this section we go the opposite way: we are given some process and we want to interpret it as the output of some unknown, approximately linear system. Before any analysis, one must reduce noisy (or nonlinear) components of the process by projecting it onto the main EOFs. Furthermore, since we assume the basic state to be fixed, we only consider anomaly processes about this state. Now, as long as the anomalies are relatively small, one can assume a *linear dynamic.* This approach can be formalized as

$$\mathbf{q}(t+1) = \mathcal{A}\mathbf{q}(t) + \text{noise}, \quad (7)$$

where $\mathbf{q}$ is our low dimensional process and the system matrix $\mathcal{A}$ is to be estimated. Note that (7) describes a first-order autoregressive process. The estimation of $\mathcal{A}$ is achieved by a simple least-squares fit via the lag 1 and lag 0 covariance matrices:

$$\mathcal{A} = (\langle \mathbf{q}_i(t+1)\mathbf{q}_j(t)\rangle)(\langle \mathbf{q}_i(t)\mathbf{q}_j(t)\rangle)^{-1}. \quad (8)$$

The POPs are defined to be the normalized eigenvectors of $\mathcal{A}$. Note that, as long as the process $\mathbf{q}(t)$ is real, the matrix $\mathcal{A}$ will also be real.

Like normal modes, POPs are real or occur in complex conjugate pairs. By expanding the state $\mathbf{q}(t)$ in the basis set consisting of these n patterns, as is done in (2) for the modes, one can derive the evolution of a POP. The evolution of such a POP is "better" the less damped it is since otherwise more noise is needed to excite the POP. For a complex POP, such good quality can also be measured by the coherence of its complex coefficient. If real and imaginary parts show at the POP period a large squared coherency at a phase lag of $\pi/2$, then this POP's evolution is close to its ideal undisturbed form. Of course, to be useful the POP should explain a significant amount of the variability of the process.

The dynamical flavor of the POPs is reflected in the fact that in (8) two time steps are coupled. As a consequence it appears that the system matrix $\mathcal{A}$ is generally no longer symmetric and the full system of POPs is not orthonormal, unlike EOFs. In extreme cases this can induce problems in discriminating between distinct POPs (see Blumenthal 1991).

The picture we get is the following: we are given a stationary process that is the output of some dynamical system. This system acts, around some equilibrium point, approximately linear. The modes of the system (the POPs) are constantly excited by the unresolved exterior noise and then damped out.

4. Problems with standing oscillations

For the following we introduce two quantities that are associated with any multivariate process: given such a process $\mathbf{q}$ (for example, the evolution of a pressure field) at a certain time t, the *intensity* of $\mathbf{q}(t)$ is measured by its geometrical *norm* $|\mathbf{q}(t)|$. At a different time t', $\mathbf{q}$ has changed to $\mathbf{q}(t')$. The amount of change can be measured by the geometrical *angle* between $\mathbf{q}(t)$ and $\mathbf{q}(t')$. The states are completely different if they are orthogonal.

With these notions in mind we again go through the cycle (6) with the process $\mathbf{m}^R(t)$ for some complex mode $\mathbf{M}$. As it is prescribed in (5R), $\mathbf{m}^R(t)$ passes more or less different patterns with varying intensity. In fact, since $\mathbf{m}^R(t)$ evolves like a spiral in a two-dimensional space there are always orthogonal, that is, totally different patterns occupied at certain distinct times. If all the patterns are of nearly equal intensity we would interpret the mode as a *traveling feature.* Note that, since all this happens in the *state space,* this does not imply that the spatial appearance of $\mathbf{m}^R(t)$ must be different.

In the opposite case, when the intensity undergoes large changes this behavior would appear as a *standing feature,* because the only thing that really happens is the oscillation between one pronounced pattern and its negative. In the extreme case, when the intensity reaches zero, the evolution equation (1) tells the zero state only to *stay at zero* since the linearity of the system demands $\mathbf{q}(t+1) = \mathcal{A}\cdot 0 = 0$. Thus, once it has reached zero, a linear system can never leave zero. So we conclude that *a linear first-order system is unable to model standing oscillations.*

We can restate the above quantitatively. We consider some mode $\mathbf{M}$ with the eigenvalue $\lambda = \rho e^{i\omega}$. For simplicity we let $\rho = 1$. The mode spiral becomes an ellipse, as Fig. 1 shows. From this ellipse we learn that it is possible to represent the mode evolution $\mathbf{m}^R(t)$ as the sum of a pure standing and a pure traveling oscillation,

$$\mathbf{m}^R(t) = \mathbf{m}^R_\sigma(t) + \mathbf{m}^R_\tau(t). \quad (9R)$$

As $\mathbf{m}^I(t) = \mathbf{m}^R(t - P/4)$ the same is true for the imaginary part:

$$\mathbf{m}^I(t) = \mathbf{m}^I_\sigma(t) + \mathbf{m}^I_\tau(t). \quad (9I)$$

We denote the amplitudes of $\mathbf{m}_\sigma(t)$ and $\mathbf{m}_\tau(t)$ by a_σ and a_τ, respectively (see Fig. 1). It is clear that a_τ equals

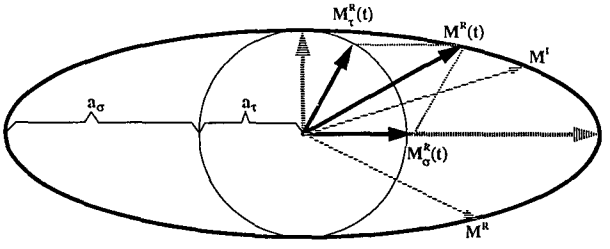

FIG. 1. The pure standing and traveling oscillations as part of an undamped mode. $\mathbf{M}^R(t)$ [text: $\mathbf{m}^R(t)$] is running through the ellipse, obeying (5R). The main axes of the ellipse are shown by the dashed thick arrows, together with a cycle that has as a radius the smaller axis. The parallel of the larger axis through $\mathbf{M}^R(t)$ intersects the cycle in a point $\mathbf{M}_\tau^R(t)$. While the process $\mathbf{M}_\tau^R(t)$ is running uniformly through the cycle, thereby describing a traveling feature of constant intensity a_τ, the process $\mathbf{M}_\sigma^R(t) = \mathbf{M}^R(t) - \mathbf{M}_\tau^R(t)$ performs a standing oscillation with amplitude a_σ. The traveling rate $\tau_\mathbf{M}$ of $\mathbf{M}$ is defined by the ratio of a_τ and the maximum intensity $a_\sigma + a_\tau$. As the traveling rate of M increases, the eccentricity of the ellipse decreases, and the ellipse becomes more circular.

the minimum intensity of the mode, while $a_\sigma + a_\tau$ equals its maximum intensity. We define:

$$\text{the } \textit{standing rate} \text{ of } \mathbf{M}\text{: } \sigma_\mathbf{M} = \frac{a_\sigma}{a_\sigma + a_\tau},$$

$$\text{the } \textit{traveling rate} \text{ of } \mathbf{M}\text{: } \tau_\mathbf{M} = \frac{a_\tau}{a_\sigma + a_\tau}.$$

In the Appendix it is shown that the system matrix $\mathcal{A}$ and the traveling rate τ_M are linked through the following relation:

$$|\sin(\omega)| \leqslant (\|\mathcal{A}\| + 1)\tau_\mathbf{M}, \tag{10}$$

where $\|\mathcal{A}\|$ denotes the matrix norm of $\mathcal{A}$.

Mathematically, this is nothing more than a (cryptically written) tautology. But physically it expresses the fact that the presence of standing oscillations is only possible at the expense of a large $\mathcal{A}$ (in terms of its norm). As a consequence we find that in the limit of a pure standing mode ($\tau_M = 0$) the mode frequency ω is forced to vanish, which means that this mode cannot oscillate.

If one is working in an EOF-truncated space one can give an explicit bound on each mode frequency (see Appendix). It depends only on n (the number of retained EOFs), $\bar{\sigma} = \sum_i \sigma_i / n$ (their average deviation), and $\sigma_{\min}^2$ (the smallest EOF variance) via the following relation:

$$\sin(\omega) \leqslant \left(\frac{\bar{\sigma} n}{\sigma_{\min}} + 1\right)\tau_\mathbf{M}. \tag{11}$$

To get a rough idea of what (11) expresses, let us suppose we are given a process that has a mean standard deviation of $\bar{\sigma} = 1$, and we project this process onto the first four EOFs. Suppose further that the fourth EOF component has a standard deviation of 0.7. Hence, in that case we roughly would find $\sin(\omega) \leqslant 7\tau_M$. Consequently, a mode with a traveling rate of 5%, say, cannot have a frequency that is higher than $\arcsin(0.35) \approx 0.35$, which corresponds to a period of 18 time steps.

Presumably it is not hard to give sharper bounds on the right-hand side of (10). But we wanted to emphasize that *a bound exists at all* that depends only on the relative variances of the EOFs. We did not mention the impact of a noisy environment on the estimation of the modes. If, for instance, a mode has such a strong standing behavior that its minimum intensity, a_τ, is comparable to the noise amplitude, then this mode is hard to detect.

5. The conjugate process: Complex time series

In the former section, we have seen that the building blocks of linear models are *cycles* (or ellipses) rather than single oscillations. This fact is, or at least should be, automatically satisfied for models that are inspired by physical reasoning. But for the purpose of fitting a model to data, as in the POP analysis, one will encounter trouble when this cycle condition is not taken care of.

The physical meaning of this condition can be explained as follows. In the moment when one of the two cyclic components passes equilibrium, the second component becomes active; it serves as a drive or *momentum* for the first. A quarter-period later the components have taken opposite roles: the second component, which now is zero, is driven by the first, which is at a maximum, and so on.

Hamiltonian mechanics has this dichotomy incorporated into its foundations since, for each degree of freedom, one always considers two "conjugate" components, location and momentum, which build up a $2n$-dimensional phase space. This is another way of expressing that Hamiltonian mechanics is of *second order*. This can be contrasted with fluid mechanical theories, which are usually of *first order* and do not show this predetermined splitting of variables. Hence, such a system can only describe oscillations because the role of the conjugates can be played by the variables themselves.

The dichotomy that we just described must be taken into account by POP analysis. Before approaching a process via the linear system approach, (1), one must ensure that the variables are *closed* with respect to *conjugacy*. Otherwise it is possible that conjugate information gets lost, for instance, when the system space is *truncated*. This often takes place, nevertheless, since the data are usually passed through a cascade of filtering operations and projections. If, for instance, we had a process that develops between two EOF patterns, one of which has only a small amplitude, then the POP analyst could overlook this oscillation simply because of the EOF truncation. Or if one investigates, say, the SST evolution at some region, one might erroneously

leave out the atmospheric wind data or some other region of the globe where the signal moves when the original SST signal is small or zero.

It is clear that this is impossible for traveling features. Here, each quarter-period, the process passes geometrically orthogonal patterns with nearly the same intensity, so the process is cyclic by definition. In such cases a POP analysis should not encounter any problems. But as a process tends toward a standing oscillation (thereby losing conjugate information) POP analysis runs into trouble. In these cases the analysis is bound to resolve a *real, nonoscillating POP,* in accordance with (10).

The most natural way of restoring approach (1) is the following. Once we have lost the conjugate components, why should we not reintroduce them? Given a process $\mathbf{q}$ we must define a priori what we now call the *conjugate process* $\mathbf{p}$. The new vector of state will be the pair $(\mathbf{q}, \mathbf{p})$ or, more appropriately to our context, the *complex state vector* $\mathbf{q} + i\mathbf{p}$.

For continuous processes the notion of conjugacy is well defined via the time derivative. For discrete processes, however, which do not know a time derivative, one faces a certain vagueness of the notion of conjugacy.

An ad hoc approximation of the time derivative would be the term $\mathbf{p}(t) = \mathbf{q}(t + 1) - \mathbf{q}(t)$. This approach is equivalent to considering second-order, instead of first-order, autoregressive processes in (7), and it tends to overemphasize the high frequencies. In the following we describe a very natural way of constructing the conjugate process.

Given $\mathbf{q}$, we switch into the frequency domain, shift the phase of $\mathbf{q}$ by $\pi/2$, and switch back into the time domain. This procedure is known as *the Hilbert transform.* Formally, for a process $\mathbf{q}(t)$ the Fourier transform $\mathbf{Q}(\omega)$ is given by

$$\mathbf{Q}(\omega) = 1/2\pi \cdot \int_{-\infty}^{\infty} \mathbf{q}(t) e^{-i\omega t} dt.$$

The tranformation

$$\mathbf{Q}^h(\omega) = \begin{cases} i \cdot \mathbf{Q}(\omega), & \omega < 0 \\ 0, & \omega = 0 \\ -i \cdot \mathbf{Q}(\omega), & \omega > 0 \end{cases} \tag{12}$$

gives the Hilbert transform $q^h(t)$ of $q(t)$ as the inverse Fourier transform of $Q^h(\omega)$, that is, by letting

$$\mathbf{q}^h(t) = \int_{-\pi}^{\pi} \mathbf{Q}^h(\omega) e^{i\omega t} d\omega. \tag{13}$$

Since the complex process $\mathbf{z} = \mathbf{q} + i\mathbf{q}^h$ essentially consists of the Fourier components of $\mathbf{q}$ one might call it the "complexification" of $\mathbf{q}$.

We now define $\mathbf{p} = \mathbf{q}^h$. The new vector of state becomes

$$\mathbf{z}(t) = \mathbf{q}(t) + i\mathbf{p}(t), \tag{14}$$

and it is an element of an n-dimensional *complex phase space.*

The Hilbert transform is a rather simple way of receiving conjugate information and appears as a kind of a "deus ex machina." However, the price we have to pay for this rescue is the indeterminateness of $\mathbf{p}$ *at time* t, since one needs future information to calculate $\mathbf{p}(t)$ exactly [see $\mathbf{Q}^h$ in (12) and (13)]. Not surprisingly, for prediction purposes (see the last section) this becomes a serious problem.

It is interesting to note that the Hilbert transform has been introduced into the geophysical literature in order to extend classical EOFs to complex EOFs (CEOFs), which are capable of resolving traveling features—see Barnett (1983) or earlier Wallace and Dickinson (1972). In just the opposite way complex POPs (CPOPs), which are to be introduced now, extend POPs in order to incorporate standing features.

6. Complex POP analysis and CPOPs

The CPOP analysis works like a full analog to POP analysis but deals exclusively with *complex processes.* Suppose we are given some process $\mathbf{q}(t)$. At first we form the conjugate process $\mathbf{p}(t)$ and the complex process $\mathbf{z}(t) = \mathbf{q}(t) + i\mathbf{p}(t)$. We interpret $\mathbf{z}(t)$ as being the output of an approximately linear system $\mathcal{S}$, but now $\mathcal{S}$ is no longer real but a *complex linear system of first order.* We use the approach

$$\mathbf{z}(t + 1) = \mathcal{C}z(t) + \text{noise}, \tag{15}$$

where $\mathcal{C}$ is now a *complex matrix.* Standard least-squares fitting yields the system matrix estimate [cf. (8)]

$$\mathcal{C} = (\langle \mathbf{z}_i(t + 1)\mathbf{z}_j^*(t) \rangle)(\langle \mathbf{z}_i(t)\mathbf{z}_j^*(t) \rangle)^{-1}, \tag{16}$$

which is now a *complex matrix* (the asterisk denoting complex conjugation). The CPOPs are defined to be the n eigenvectors $\mathbf{C}_1, \ldots, \mathbf{C}_n$ of $\mathcal{C}$ supplied with eigenvalues $\lambda_1, \ldots, \lambda_n$. They are usually linearly independent, thus we can uniquely expand the complex state $\mathbf{z}(t)$ in terms of the CPOPs, yielding

$$\mathbf{z}(t) = \gamma_1(t)\mathbf{C}_1 + \cdots + \gamma_n(t)\mathbf{C}_n; \tag{17}$$

$\gamma_j(t)$ is called the CPOP coefficient of CPOP $\mathbf{C}_j$. It determines the time evolution of the CPOP. For a given CPOP $\mathbf{C}$ with eigenvalue λ (dropping the index) we may write $\lambda = e^{-1/\tau} \cdot e^{i\omega}$, which gives us the two characteristic times for $\mathbf{C}$: the *period* $P = 2\pi/\omega$ and the *e*-folding (decay) time τ. The complex pattern $\mathbf{C}$, its time coefficient $\gamma(t)$, and the characteristic times P and τ determine the CPOP completely.

Note that as for POPs, the state of a CPOP is not given by a simple projection. Since CPOPs usually do not form an orthonormal system, the state depends on all other CPOPs.

The CPOP process is given by the multivariate complex time series $\mathbf{c}(t) = \gamma(t)\mathbf{C}$. It reads in the location $\mathbf{q}$ space

$$\mathbf{c}^{\mathrm{R}}(t) = \gamma^{\mathrm{R}}(t)\mathbf{C}^{\mathrm{R}} - \gamma^{\mathrm{I}}(t)\mathbf{C}^{\mathrm{I}}, \qquad (18\mathrm{R})$$

and in the momentum $\mathbf{p}$ space:

$$\mathbf{c}^{\mathrm{I}}(t) = \gamma^{\mathrm{R}}(t)\mathbf{C}^{\mathrm{I}} + \gamma^{\mathrm{I}}(t)\mathbf{C}^{\mathrm{R}}. \qquad (18\mathrm{I})$$

The amount of explained variance of a (C)POP can be measured by the term $1 - \epsilon^2/v^2$, where ϵ^2 and v^2 denote the variance of the error $\mathbf{c}^{\mathrm{R}}(t) - \mathbf{q}(t)$ and process $\mathbf{q}(t)$. It is normally given in percentages.

If there were no noise in the system the evolutions (18) would describe a pure mode of the form (5). In the presence of a noisy energy input, however, the system's modes are constantly excited to perform their genuine oscillations. These motions are recognized as the CPOPs of the system.

Now there are *two* cycles that belong to a CPOP, the $\mathbf{q}$ cycle and the $\mathbf{p}$ cycle, which run through the same patterns but with a lag of a quarter-period:

$$\begin{array}{ccccccccc} \mathbf{q}: & \mathbf{C}^{\mathrm{R}} & \longrightarrow & -\mathbf{C}^{\mathrm{I}} & \longrightarrow & -\mathbf{C}^{\mathrm{R}} & \longrightarrow & \mathbf{C}^{\mathrm{I}} & \longrightarrow & \mathbf{C}^{\mathrm{R}} \\ & \downarrow & & \downarrow & & \downarrow & & \downarrow & & \downarrow \\ \mathbf{p}: & \mathbf{C}^{\mathrm{I}} & \longrightarrow & \mathbf{C}^{\mathrm{R}} & \longrightarrow & -\mathbf{C}^{\mathrm{I}} & \longrightarrow & -\mathbf{C}^{\mathrm{R}} & \longrightarrow & \mathbf{C}^{\mathrm{I}}. \end{array} \qquad (19)$$

Because an n-dimensional process has n degrees of freedom the CPOP model is able to resolve n independent oscillations. This is in contrast to the POP approach, which prescribes the number of oscillatory degrees of freedom to be at most $n/2$. We will come back to this point in the next section.

7. Testing the CPOPs

a. With synthetic data

In order to test whether CPOP analysis works correctly, we produced a series of low-dimensional complex autoregressive processes of first order with prescribed modes. This can be achieved by forming the diagonal matrix Λ, the entries being the prescribed eigenvalues, and the matrix $M = (\mathbf{M}_i)$, with $\mathbf{M}_i$ denoting the sequence of the prescribed eigenvectors. Forming the complex matrix $\mathcal{C} := M\Lambda M^{-1}$, we can create the complex autoregressive process of first order [see (15)]

$$\mathbf{z}(t+1) = \mathcal{C}\mathbf{z}(t) + \text{noise},$$

where "noise" denotes some complex white noise process. This z will then have the desired modes. Note that such a process without any damping or noise would be equivalent to a superposition of waves of the form (5) with $\rho = 1$.

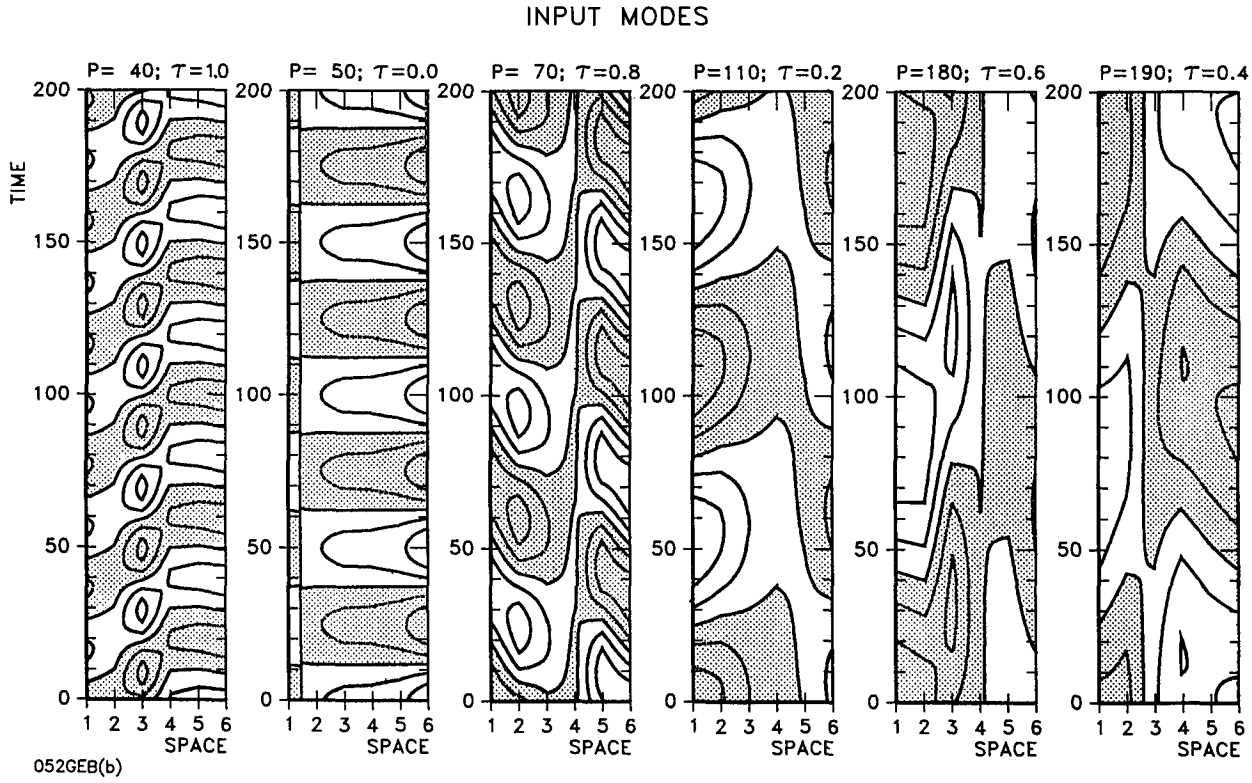

FIG. 2. The six independent synthetic input modes in a Hovmoeller diagram. They were used as the undamped modes of a six-dimensional complex linear process. Shaded areas indicate negative values. Note the varying traveling rates of the modes.

We used a set of six independent modes in a six-dimensional complex space. The real part, $\mathbf{q}(t)$, of the complex process $\mathbf{z}(t) = \mathbf{q}(t) + i\mathbf{p}(t)$ was then subjected to a CPOP analysis. Figure 2 shows a case without any damping and noise, and with traveling rates $\tau = 0$, 0.2, 0.4, 0.6, 0.8, and 1.

In order to avoid similar harmonics of the modes we chose the periods to be relatively rationally independent (i.e., they have no large common divisors). This has the consequence that each single wave becomes more invisible in a superposition of the six.

The CPOPs that were resolved are shown in Fig. 3. There is obviously no significant difference between the six modes and the CPOPs.

We already mentioned that a POP analysis can resolve at most half of the maximum number of oscillations. Hence, in this case there can only be three complex POPs, the number that we actually found. They are shown in Fig. 4. One sees that the three POPs are only of minor descriptive value. The first two POPs show a traveling feature with a certain regularity, but there is no significant resemblance to any of the input modes.

From this analysis we can learn two things: first, that a real process of dimension n is, in fact, able to comprise n independent waves of the form (5R) as modes. These modes, however, are not modes of an n-dimensional real linear system but of an enlarged linear system that incorporates and models the momentum of the system. CPOP analysis proves that it is possible to recover these modes from the system's (real) state evolution alone. Second, if there is such a process with a maximal number of waves then a usual POP analysis would resolve at most half as many complex POPs. Hence, the procedure is bound to mix two (or more) modes into one POP, with the consequence that this POP cannot evolve as regularly as it should.

Of course, in addition to being rather academic these conclusions are grounded in only one (or one type of) example, so they must be taken with some caution.

b. *With an ENSO process*

To test the CPOP model further and to compare the results with the POP model, we analyzed a time series of equatorial monthly SST anomalies. This time series is a composition of two independent series that span the Indian and Pacific oceans between 45°W and 85°E in 24 locations. The first series, which ranges from 1951 to 1986, is an updated form of the dataset described in Barnett (1983) and has already been used in Storch et al. (1990). The second series ranges from 1982 to 1991 and is an updated form of the dataset described in Reynolds (1988). In the overlapping period from

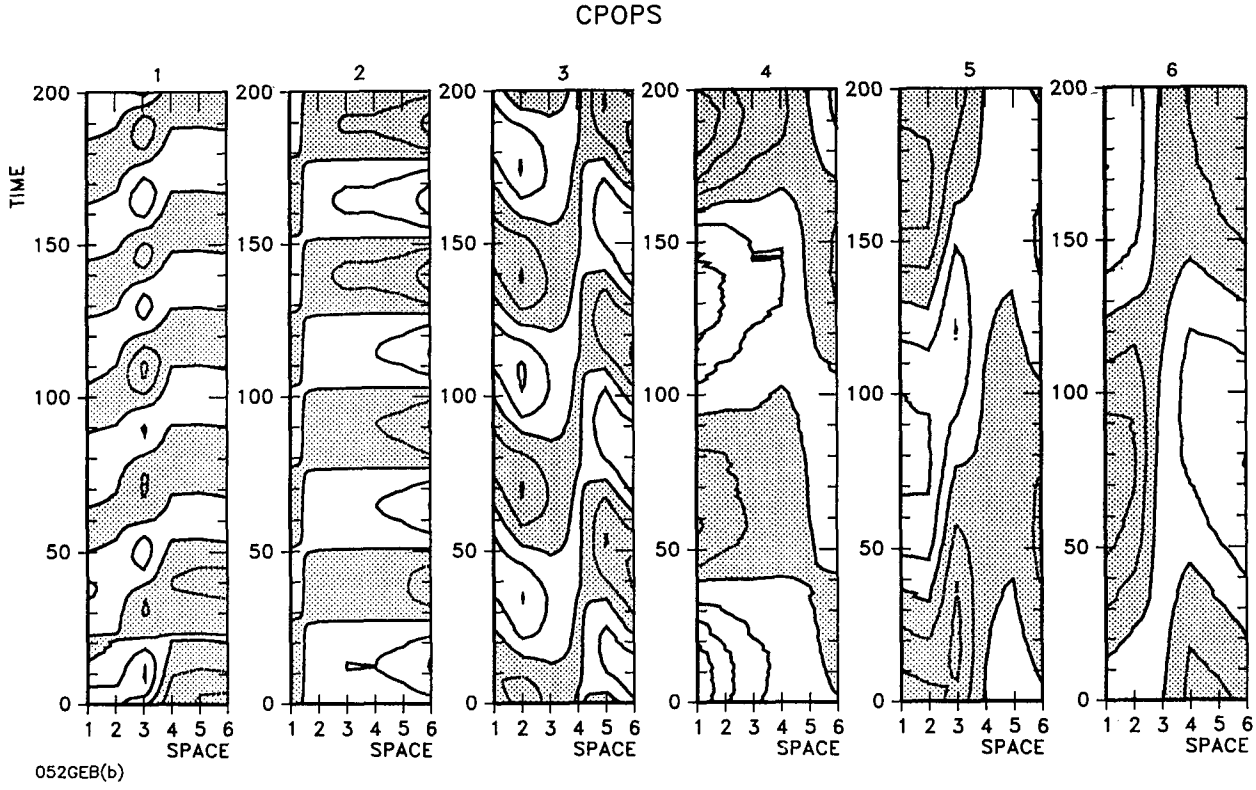

FIG. 3. The six independent CPOPs of the synthetic process shown in a Hovmoeller diagram. They reproduce the given input modes of Fig. 2 very convincingly.

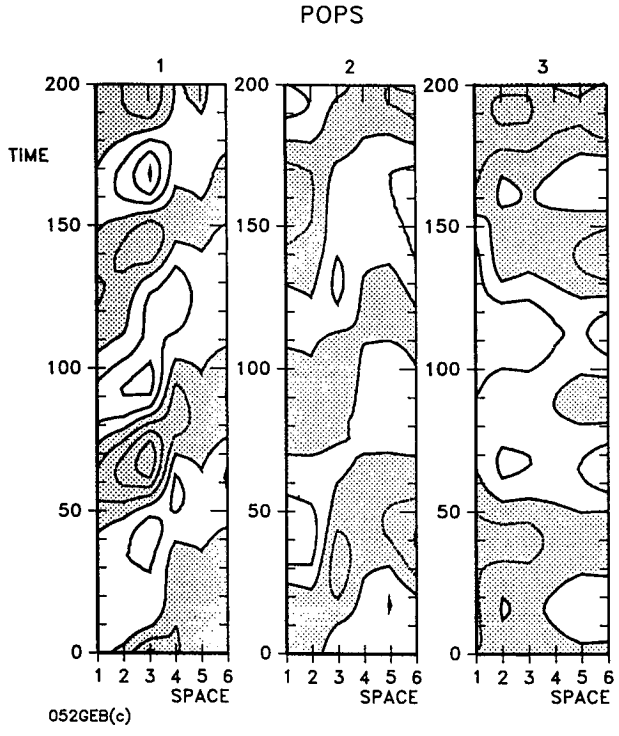

FIG. 4. The three resolved POPs of the synthetical six-dimensional process. The input modes are not detected. POP 1 could be a merging of modes 1 and 3.

1982 to 1986 a simple interpolation has been used to merge both series together.

It is well known that the dominant signal in the interannual time scale is the periodically occuring El Niño–Southern Oscillation (ENSO) phenomenon. One main feature of ENSO consists of a nearly standing oscillation in the SST anomaly field over the whole oceanic region, with centers in the mid- and eastern Pacific [see Xu and Storch (1990)]. Its period is usually estimated to 30–40 months, and there are hints that there exists a connection to the annual cycle. For the details of ENSO we refer the reader to McCreary and Anderson (1991).

Truncating the 24-dimensional SST process to the first ten EOFs retains about 90% of the variance, and there is one dominant EOF that accounts for nearly 45%. We subjected the ten-dimensional principal component time series to a POP and a CPOP analysis. The only POP that explained a substantial amount of variance (12% of the whole SST field) was complex but its coefficient did not develop very coherently, with a vague spectral peak near 30 months. The POP period was unrealistically long (86 months), which might also have been influenced by the fact that in this case the minimal resolvable period was 26 months, according to (11). CPOP analysis resolved a 36-month standing oscillation, which explains about 26% of the variance with a complex coefficient that develops coherently at that period (99% significance level). Figure 5 shows the POP and CPOP patterns (real and imaginary part) together with the dominant EOF pattern. The large amount of explained variance of this EOF (Fig. 5a) indicates that, in fact, the SST shows a nearly standing behavior. POP analysis, however, reveals a pattern pair (Fig. 5b) with a fairly large traveling rate of $\tau = 0.46$. The traveling mostly occurs between 90°E and 160°E.

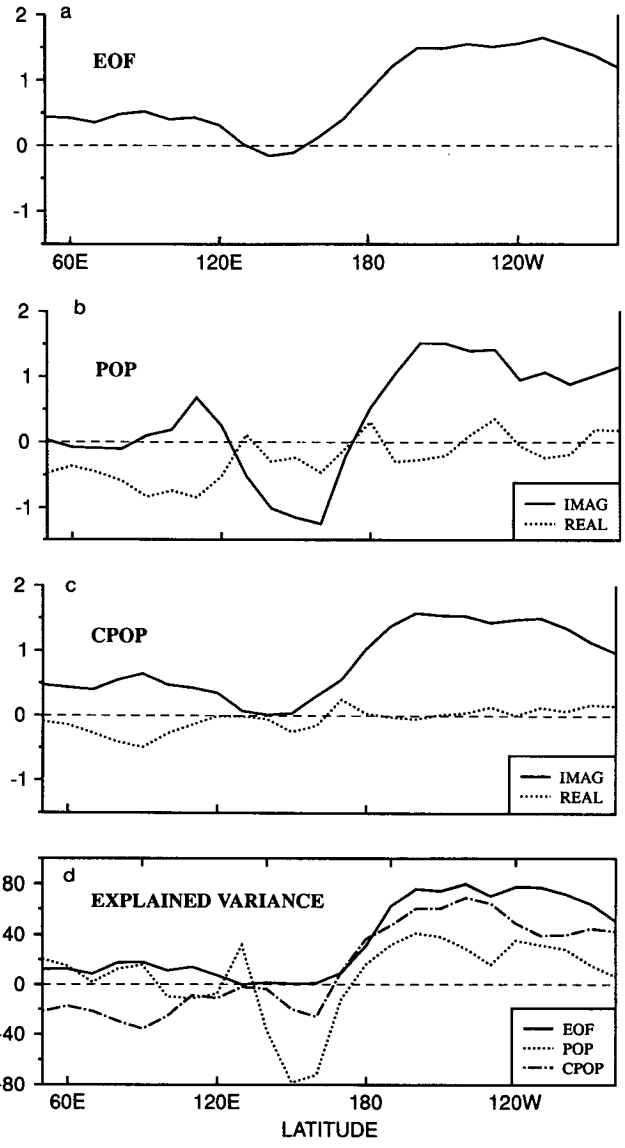

FIG. 5. The resolved ENSO pattern. (a) Dominant EOF, which explains 45% of the SST anomaly variance. It is characterized by a large SST anomaly over the whole Pacific. (b) Dominant POP. The imaginary part resembles the EOF, but has large negative values at 150°E (near Indonesia). The real part shows larger deviations from zero. (c) Dominant CPOP. Its real part has a marked similarity to the EOF, and its imaginary part is small nearly everywhere. (d) Explained variances of all patterns. For the EOF this is largest (by definition), especially over the Pacific. The CPOP explains much variance over the Pacific and is worse over the Indian Ocean. The negative values of the POP at 150°E are striking.

This is a rather poor data region since it is essentially over Indonesia. The standing SST oscillation can be seen very clearly in the CPOP process, which has a traveling rate of $\tau = 0.19$ (Fig. 5c). Its imaginary part is very similar to the first EOF, and the real part is nearly zero everywhere. By definition, the explained variance is highest for the EOF (Fig. 5d). Over the Pacific, where the oscillation is strongest, it shows values of up to 80% followed by the CPOP with values of around 60%. The explained variance of the POP merely reaches values of 40% over the Pacific, but becomes strongly negative (−80%) over Indonesia, indicating the poor results of the analysis there.

The complex POP and CPOP coefficients are shown in Fig. 6. In order to avoid the 2π jumps we depict the phase evolution in an integrated form. In other words, we substitute the original phase evolution $\phi(t)$ by the recursively defined new value $\phi'(t) = \phi'(t-1) + \phi(t)$. We see that the CPOP's amplitude as well as its phase are obviously more undisturbed by noise than the respective parts of the POP. For instance, the various ENSO events appear more clearly in the CPOP amplitude. The POP amplitude shows a lot of high-frequency noise, and it is erroneously large in the sixties. Similarly, whereas the POP phase speed shows large disturbances on long as well as short time scales, the phase speed is nearly constant for the CPOP. Note that even the strongest ENSO events do not affect the phase speed. Altogether POP and CPOP perform nearly 11 cycles during the whole period, which results in a period of 45 months, a bit longer than the CPOP period.

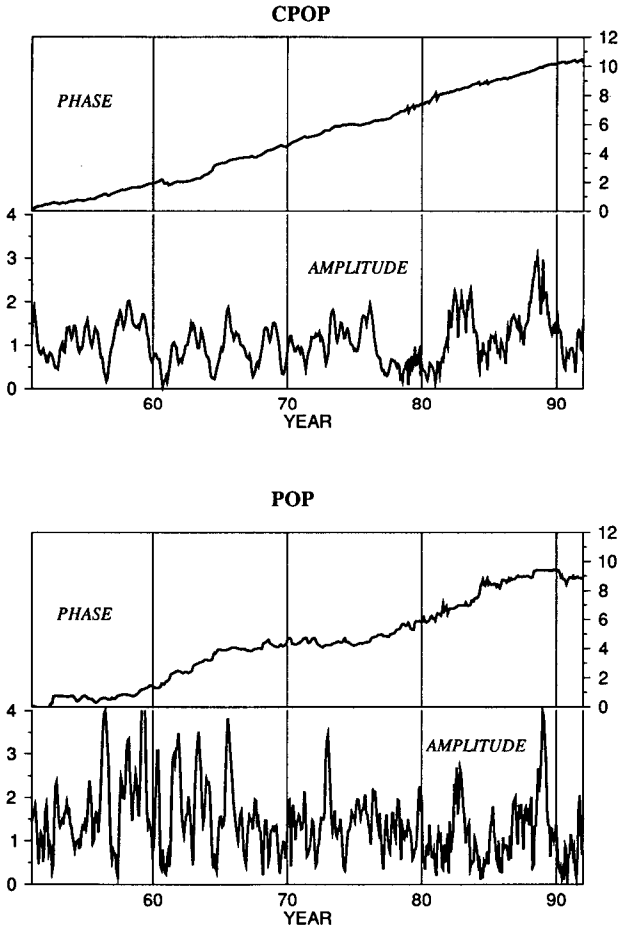

FIG. 6. Amplitude and phase plot of the (C)POP coefficient. The phase is plotted in the integrated form, that is, the 2π jumps are eliminated. Especially from the CPOP coefficient (upper panel) one sees that the various events are events of the amplitude. All important events (e.g., 1958, 1966, 1976, 1983, 1987, 1989) are well represented in the amplitude. During the events the phase is not affected at all. It shows a generic phase speed of 490/11 = 45 months cycle^{-1}. POP amplitude and phase evolution show a lot of noise. Various events (1966, 1973, 1983, 1989) appear like overshooting spikes in the amplitude. There is no clear, generic, recognizable phase speed.

The classical measure of the ENSO phenomenon is the Southern Oscillation index (SOI), which is essentially gained as an averaged value of the SST anomalies over the so-called Niño3 area in the eastern Pacific, (see Wright 1985). To compare our analysis results to the SOI we therefore averaged both, the POP and CPOP process, and also the dominant EOF process, over the corresponding equatorial section. We call the results EOF-SOI, POP-SOI, and CPOP-SOI. The result is shown in Fig. 7. With a correlation of 94% the EOF-SOI (bottom panel) resembles the SOI nearly completely. This is just another proof that the SST part of ENSO is a standing feature, describable by a single pattern and one real time series. The POP-SOI (middle panel) shares a correlation of 61% with the SOI. Especially in the fifties and sixties it is highly out of sync with the SOI. The events of 1963 and 1965 are largely overestimated, and in 1968 POP analysis even suggests a big warm event where a slight cold event was prevailing. On the other hand, the 1972 El Niño is only very poor in the POP-SOI. The performance in the 1970s and 1980s is much better, with a good representation of the large 1983 and 1987 El Niño, as well as the 1989 La Niña.

The 82% correlation of the CPOP-SOI (top panel) is mostly due to the fact that during the whole period, even in the fifties and sixties, it evolves very synchroneously to the SOI. This is natural since from the pattern one sees that the real part of the CPOP mostly resembles the dominant EOF while the imaginary part is zero. Moreover, the various warm and cold events are well represented without the large overestimates. As for the POP-SOI, only the 1957 warm event is too strong in the CPOP-SOI.

c. *With the Madden–Julian Oscillation*

For the last application of the CPOP model we chose the Madden–Julian Oscillation (MJO), see Madden and Julian (1972). The MJO is the most dominant atmospheric signal in the tropics in the intraseasonal time scale. It is a disturbance traveling eastward around

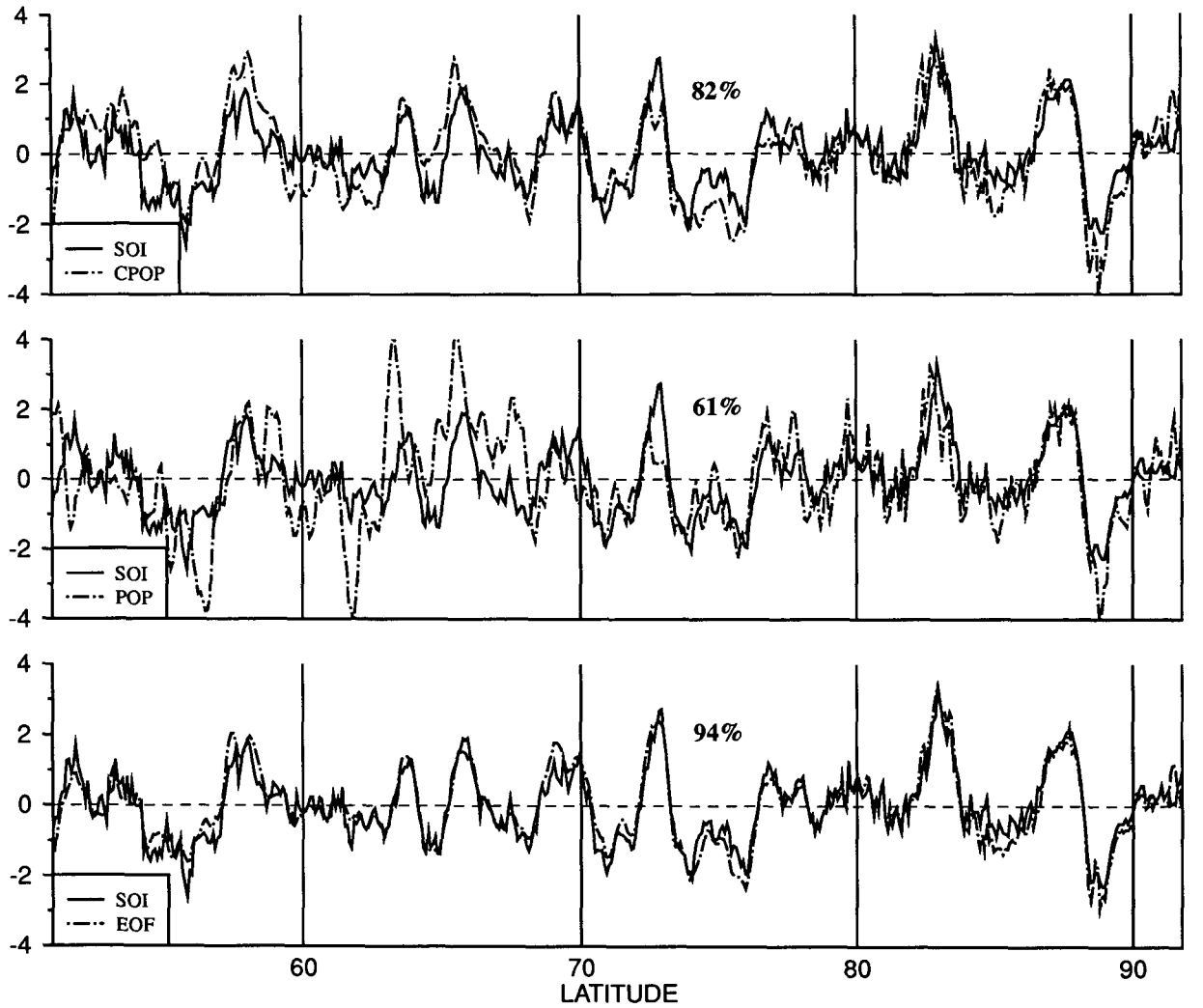

FIG. 7. SOI and reproduction of SOI by EOF, POP, and CPOP. There is no significant difference between EOF-SOI and SOI (lower panel, 91% correlation). The POP-SOI (middle panel, 61%) is uncorrelated especially in the fifties and late sixties, whereas it well represents the events of the 1960s and the 1980s. Note the large overshootings at various events. The CPOP-SOI (top panel, 81%) is generally closer to the SOI and does not have the high-frequency noise like the POP-SOI.

the globe. The MJO can be observed in the geopotential height or zonal wind of the lower troposphere and shows, in the 20°S–20°N belt, a large-scale pattern of wavenumber 1 with a pronounced structure over the Pacific. The phase speed of the MJO has considerable variability, moving relatively slowly over the Indian Ocean and much faster over other parts. The MJO shows a pronounced modulation by the annual cycle. It is much stronger during the northern winter season than in the summer.

We analyzed daily values of 850-mb zonal winds in the tropical belt between 20°S and 20°N, from 1 January 1984 to 31 December 1987. The data come from the European Centre for Medium-Range Weather Forecasts in a 10- by 5-degree resolution. To remove the annual and semiannual cycle as well as the main noise components, we processed the data in the following manner: we first calculated the 36 meridional averages and projected them onto the first ten EOFs. The principal components were then high-pass filtered with a cut period of 120 days tapered off to 180 days. The resulting ten-dimensional time series was then (C)POP analyzed.

Figure 8 shows the main resolved patterns. The two dominant EOFs explain 18% and 12%, respectively, of the whole variance of the time-filtered data (Figs. 8a and 8d). The first EOF has a small minimum near 60°E and a maximum near the date line. The second EOF has a minimum at 90°E and another smaller maximum in the east Pacific. Their principal component time series are correlated with 47%, where the first leads the second by around 11 days. This means

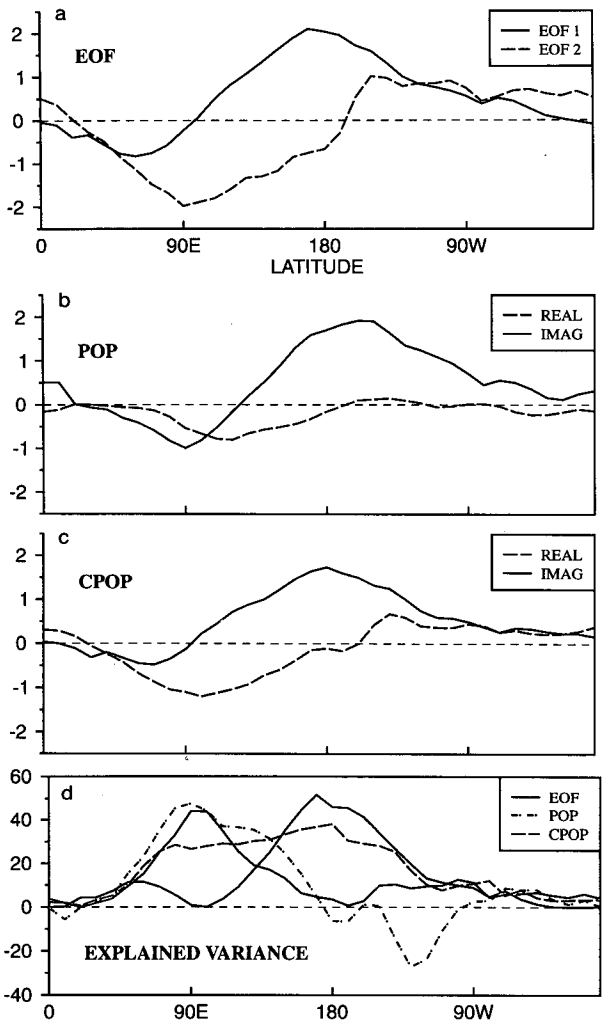

FIG. 8. Resolved pattern for the MJO. (a) First two EOFs explaining 18% and 12% of the overall variance. Cross-correlation analysis indicates that the first EOF propagates toward the second. (b) POP-wave; global wave of wavenumber 1. The wave is amplified at 60°E–90°E; its speed is considerably small there. This leads to irregularities in the POP phase evolution. (c) CPOP-wave; besides a slightly smaller amplitude, the patterns nearly completely resemble the EOF wave. From the CPOP cycle, one knows that the consecutive order is EOF 1, EOF 2, −EOF1, −EOF 2, EOF 1, etc., which determines a full global cycle. (d) Explained variance of the patterns. Note the large local values of both EOFs. Remarkable are the large negative values of the POP beyond the date line. The combination of EOF 1 and EOF 2 in the CPOP is reflected in its explained variance.

that, on average, EOF 1 travels eastward toward EOF 2.

Evoking the cycle (19), we can see in Fig. 8c that the propagation from EOF 1 to EOF 2 is part of the CPOP cycle, and is actually a global wave. Since the real and imaginary parts of the CPOP essentially resemble EOF 2 and EOF 1, respectively, we see that the complete history of this phenomenon can be described by the series

$$\text{EOF 1} \rightarrow \text{EOF 2} \rightarrow -\text{EOF 1} \rightarrow -\text{EOF 2} \rightarrow \text{EOF 1}.$$

Note that the transition from EOF 1 to EOF 2 means a large amplification of the signal between 60°E and 90°E, that is, in the Indian Ocean. Also, in this area the wave speed is about 2.3 m s^{-1}, which is considerably slower than the speed over the Pacific Ocean (about 10 m s^{-1}). The signal remains rather strong over the Pacific and then almost fades out.

The POP cycle (see Fig. 8b) essentially describes nearly the same course of events, only that the real part of the POP has a much smaller scale than EOF 2. Also, the whole POP, especially the imaginary part, is shifted toward the east by about 20°. Moreover, over Africa (~20°E) there is no signal at all, such that the wave travel is actually interrupted there. The signal reappears over the Indian Ocean and continues its travel like the CPOP wave. Note that, apart from the interruption of the POP wave over Africa, the POP as well as the CPOP wave describes a full global cycle.

The lower panel of Figure 8 shows the explained variances of the different patterns. The shape of the curves of both EOFs is very similar to the EOFs themselves. Both locally and on average, the two EOFs together show higher values than POP and CPOP, which is understandable from the definition of EOFs. The POP shows only a good performance west of the date line. Toward the east, the explained variance drops down to large negative values (up to −30%). The CPOP, however, explains a considerable amount of variance over the whole section between 60°E and 120°W, with maximum values of about 40%. The lower values of explained variance, for the POP as well as for the CPOP, compared to the EOFs is reasonable since the EOFs are optimized structures that explain a maximum amount of variance, whereas the former are optimized with the *side condition* to perform a full cycle.

The main difference between POP and CPOP analysis can be seen in their time evolution. Figure 9 shows the POP and CPOP coefficients again in an amplitude-phase diagram, from day 1 to day 500. We see that the POP amplitude is superimposed by a lot of high-frequency noise, similar to the ENSO example. The phase evolution does not show any regularity at all; it even shows the tendency to decrease, contrary to the POP model that tells the phase to increase. This behavior is difficult to interpret. But it might be explained by the fact that the two POP minima are relatively close together in an area that is dominating the POP (in terms of explained variance). Since the wave propagation there is fairly slow, this can result in a transient reversal of the phase speed. When the amplitude is strong, for instance between time steps 330 and 430, the phase speed is consistent.

Contrary to this, the CPOP phase evolution behaves much more regularly. It is constantly increasing to a final value of 49 cycles in 1461 days, which gives an average phase speed of one cycle per 30 days, in accordance with the CPOP period of 28 days. These val-

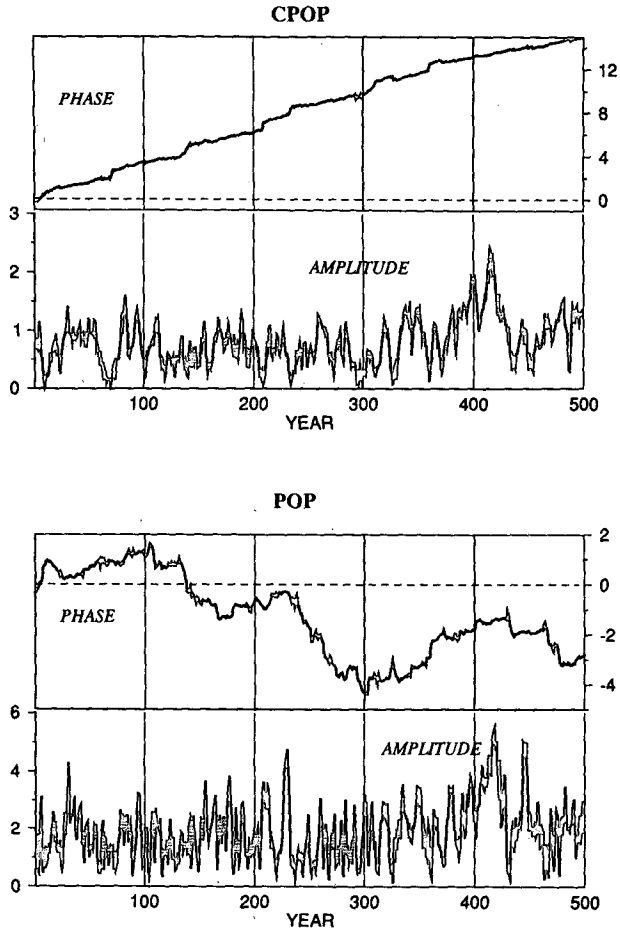

FIG. 9. Amplitude-phase diagram of POP and CPOP coefficient, from day 1 to day 500 (compare with Fig. 6). The POP amplitude (lower panel) is superimposed by a lot of high-frequency noise, similar to the ENSO example. Note the striking irregularity of the phase evolution. Only at large amplitudes (e.g., time steps 330–430) is the phase speed consistently positive. The CPOP phase evolution (upper panel) behaves much more regularly. From it one can derive an average phase speed of one cycle per 30 days. The CPOP amplitude is much more undisturbed by high-frequency noise than the POP amplitude, but it is also smaller by a factor of two.

ues lie on the lower limit of the values estimated so far (see, e.g., Madden and Julian 1972). The CPOP amplitude is much more undisturbed by high-frequency noise than the the POP amplitude, but it is also smaller by a factor of two.

After all it can be said that the analyzed data show a clear traveling feature that can be identified with the 30–60 day wave, or Madden–Julian oscillation. Both POP and CPOP analysis are able to recover the patterns of this wave, which are practically identical to the first two EOFs. However, whereas CPOP analysis is able to resolve a time behavior that is both regular on the one hand, and consistent with the findings so far on the other hand, POP analysis has greater trouble in this example. We have no explanation for why POP analysis performs so badly in this example. Perhaps the reason is related to the experience that POP analysis often needs a crude low-pass filtering to show satisfactory results. Another reason might be that the statistics of the MJO are very sensitive to the annual cycle, and this perhaps is only traced by POP analysis.

Now that CPOPs seem to evolve, at least as oscillations are considered, more regularly and more closely to the physical signals, can we hope to make better predictions with CPOPs? The serious problems we encounter here are discussed in the last section.

8. Predicting the CPOPs

We describe the CPOP prediction by applying it to the case of predicting the state of ENSO, that is, by forecasting the SOI. This scheme can never approach the skill of fully-coupled model predictions that are currently in use, since we are dealing merely with a small linear model that incorporates no physics at all.

Each prediction scheme tries, at a certain time t, to determine the value $x(t+\tau)$ of the *predictand* x from the value $\xi(t)$ of the *predictor* ξ, with τ being the prediction lag. In our case, the predictor ξ is given by the coefficient of the dominant CPOP C, and the predictand x is the SOI. As our prediction scheme does not differ from the conventional POP scheme we do not go into the details, which have been described comprehensively by Xu and Storch (1990). The main step of the prediction is to forecast the CPOP coefficient by means of the eigenvalue λ, according to Eq. (4),

$$\xi(t+\tau) = \lambda^{\tau}\xi(t). \tag{20}$$

From $\xi(t+\tau)$ we form the Niño3 average of $c(t+\tau) = \xi(t+\tau)C$ and compare the result to the SOI. Doing this for each time t we can calculate the corresponding correlation skill of the forecast. So far, there is no difference between the POP and the CPOP prediction scheme. It is at the very beginning of the prediction procedure that the CPOP scheme is much more involved.

Once a system of POPs is given, the state of a POP (its coefficient) is determined via (2) and is only dependent on the state of the process $q(t)$. The state $\gamma(t)$ of a CPOP, however, is determined via (17) by $z(t)$, which is composed of the original $q(t)$ and the conjugate $p(t)$. But the value $p(t)$, which is given by (13), depends on the whole process q. For $\gamma(t)$ to be *the state at time t* this is reasonable only if $p(t)$ is approximately determined within at least some neighborhood of t. Realizations of the Hilbert transform by linear numerical filters (see Brillinger 1975) show that this is in fact the case, but only if the filter coefficients are antisymmetric about each time t. In other words, the concrete determination of p at some given time depends on future information which, of course, undermines any sort of prediction.

The time–antisymmetry condition is directly coupled to the frequency–antisymmetry of the Hilbert transform in (12), and one cannot violate the first condition without violating the second. Hence, there is no linear numerical filter that is both causal, that is, needs no future information, and is also a good approximate to the Hilbert transform.

Nevertheless, there is a causal procedure that grows directly out of the CPOP analysis. The only thing that is needed is a complex linear model $\mathcal{C}$ of the form (15). The transformation is done in the following way: given a process q we want to find a *causal* approximation of the Hilbert transform $p = q^h$, which we denote p_c. So suppose we are given $q(t)$ where t ranges from $t = 1$ until $t = today$. What is $p_c(today)$? We already know that (15) controls the evolution of the complex time series $z = q + ip$. Writing (15) explicitly we have

$$q(t+1) + ip(t+1) = \mathcal{C}(q(t) + ip(t)) + \text{noise}.$$

■ ■ * ■ ■

(21a)

The box indicates the *known parameters* and the star the *unknown variables* of the minimization procedure for CPOP *analysis*. Now we interchange the roles of $\mathcal{C}$ and p,

$$q(t+1) + ip(t+1) = \mathcal{C}(q(t) + ip(t)) + \text{noise}.$$

■ * ■ ■ *

(21b)

This is the configuration in CPOP *prediction:* $\mathcal{C}$ has become a known parameter and p an *unknown variable*. Like q, p ranges from $t = 1$ up to $t = today$, and this can be a huge number of variables. Nevertheless, the new variables p occur linearly in (21); hence the noise-minimizing solution is uniquely determined, as it was in the analysis approach for the matrix $\mathcal{C}$ with the expression (16). We find a value $p(today)$ and we let $p_c(today) = p(today)$, calling p_c the *causal conjugate process*.

It may be a bit confusing that for the p above one does not necessarily have $p_c(today - 1) = p(today - 1)$. This is because each "today" has its own minimization procedure for the determination of $p_c(today)$. Among other things, this means that the transformation $p \mapsto p_c$ is nonlinear. The causal conjugate process is, therefore, a very involved notion and, from an esthetic or physical point of view, not very satisfying. On the other hand, thinking of the conjugate process as bearing tendency information of the system it appears natural that its determination is not simple in the absence of future information. However, in our example the causal and the noncausal CPOP coefficient showed a complex correlation of 91%, a satisfactory affirmation that the approximation was quite good.

Since the CPOP model (pattern and eigenvalue) was estimated from the predictand time series, we actually make hindcast experiments. Real forecast experiments become reasonable only if the time series under consideration is significantly longer.

Let us now summarize the procedure. At first we calculate the causal conjugate process p. From this we determine, via (14) and (17), the complex process z and the coefficient ξ of the CPOP in question. Then we apply the prediction scheme (20). The corresponding lag statistic is shown in Fig. 10.

One sees that CPOP prediction is better than persistence for lags $\geqslant 3$, and with respect to the 40% level it leads persistence by about four to five months. As a reference, we also plotted the POP forecast skill. It is not of great value since the rather poor initial correlation of 61% to the SOI is already much too low.

A final remark; to predict ENSO we relied only on the equatorial SST, which showed a standing oscillatory pattern. For the linear model to work correctly we had to add conjugate information, and we did so by introducing the Hilbert transform as the conjugate process.

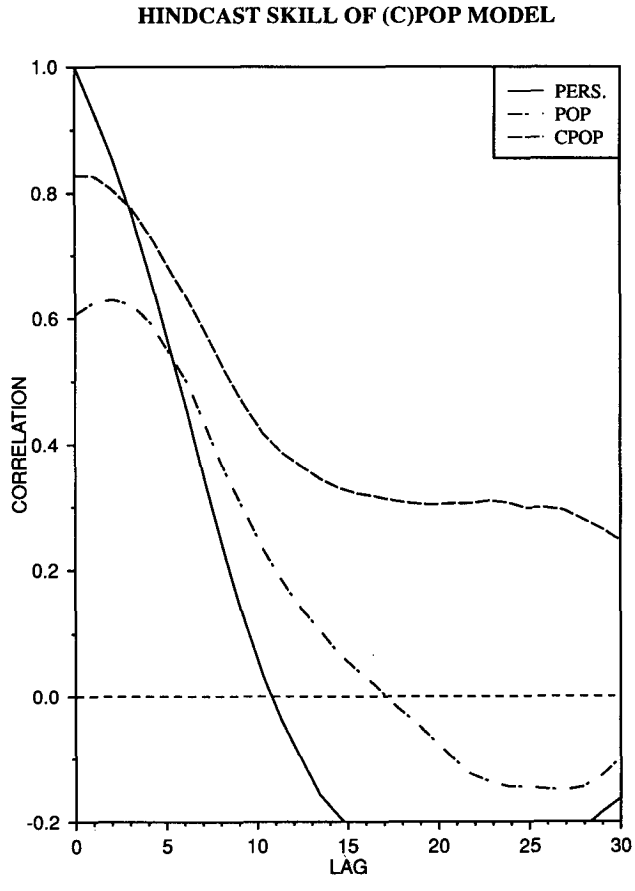

FIG. 10. The skill for the (C)POP forecast scheme compared with the SOI persistence forecast. At the 40% level, the POP forecast beats persistence by one month, and the CPOP beats the POP by nearly 3.5 months. The main reason lies in the big difference in the initial correlation.

But, of course, the enlarged complex process (14) contains the same amount of information as the original one. If important parts of ENSO truly act linearly, then to complete the cycle, there should exist such a conjugate process of the SST *in nature,* a process that furthermore would bear additional information and that could improve the predictions. In fact, this conjugate quantity exists as the heat content of the equatorial ocean, and its predictive skill has been described by Latif et al. (1993).

9. Conclusions

As a new tool for the resolution of regular evolving patterns from a field process with many degrees of freedom we have introduced the complex principal oscillation pattern analysis. It is a direct extension of the real POP analysis into the complex domain. We have shown that this extension is necessary in order to handle oscillations adequately. Physically, this results in an a priori introduction of the system's momentum analogous to Hamiltonian mechanics. The CPOPs, which are the modes of the complex linear model as estimated from the data, turn out to be more regular and predictable than POPs, at least in our three examples. Theoretically, the extension to CPOPs is redundant for traveling features or if the system is not truncated. In these cases the momentum is hidden in the process itself. But in our example of the MJO, CPOP analysis resolved a wave that looked much more regular than the corresponding POP wave.

CPOP analysis is capable of resolving any kind of oscillation, whether traveling or standing. At dominant frequencies it extracts a generic pattern pair and describes the damped cyclic evolution between these two patterns, excited by noise. In this way CPOP analysis is a very concise method of representing the information that is held in the complete cross-spectral matrix of a process.

We cannot exclude that some of the regularity of a CPOP process is artificial. Of course, we can represent any process as a superposition of arbitrary regular "modes" if there were no limit on their number, like in the Fourier theorem. But this would certainly decrease the amount of explained variance of each of them. Hence, as long as there is no clear definition of something like "subprocess" we are free to choose anything that behaves regular and explains a certain amount of variance. Both conditions are satisfied for CPOPs, at least as far as our experiments show. Moreover, they inherit the dynamical flavor from the POP model. Thus, if we want to emphasize the dynamical aspects of a process we would prefer POPs or CPOPs. If we are only interested in an optimal representation of a dataset *at one time* (such that, for instance, any permutation of time steps would lead to same result) then EOFs (or SVDs or CCAs) are recommended.

The many other complex and extended EOF analysis techniques take an intermediate position in this respect. We might call these approaches kinematical, since on the one hand one must depend on the ordering of time, but on the other hand there is no dynamical model. The relationship between these techniques and CPOPs should be analyzed more closely. Perhaps in that way one may even find an analysis technique that shares the elegance and simplicity of EOFs, the dynamical flavor of POPs, and the ability to resolve oscillations of any kind.

Acknowledgments. First of all I would like to thank Hans v. Storch and Mojib Latif. Both have been most involved in the material given above, the former more in his positive and encouraging comments, and the latter more in his very helpful critical remarks which then were encouraging, too. The same with Reiner Schnur; without him all this stuff could not have been squeezed into the computer. After the paper's completion, Grant Branstator joined our institute. His very helpful critique made me write the paper a second time. This work was made possible by the generous support of the Max-Planck Institut für Meteorologie, Hamburg, Germany.

APPENDIX

The Bounded Mode Frequency

Suppose we are given a linear system matrix $\mathcal{A}$, one of its modes M with eigenvalue $\lambda = \rho \cdot e^{i\omega}$. We know that the mode evolution $m(t)$ can be decomposed into a pure standing and a pure traveling part. At a certain time, t_0, the standing oscillation passes its maximum. Since for each t, $m(t)$ is also an eigenvector of $\mathcal{A}$, we can apply the eigenequation to $m(t_0)$. It reads for the imaginary part:

$$[\mathcal{A} - \cos(\omega)]m^{\mathrm{I}}(t_0) = \sin(\omega)m^{\mathrm{R}}(t_0). \quad \text{(A.1)}$$

Let $\|\mathcal{A}\|$ be the induced matrix norm for which $|\mathcal{A}x| \leq \|\mathcal{A}\|\,|x|$ holds. That is, abstractly, $\|\cdot\|$ can be defined as the supreme of $|\mathcal{A}x|\,|x|^{-1}$, with x running over the unit ball. Thus, we may write

$$|\sin(\omega)| \leq \|\mathcal{A} - \cos(\omega)\| \frac{|M^{\mathrm{I}}(t_0)|}{|M^{\mathrm{R}}(t_0)|}. \quad \text{(A.2)}$$

The denominator in the above expression equals $a_\sigma + a_\tau$. Evoking the relation $m^{\mathrm{I}}(t_0) = m^{\mathrm{R}}(t_0 - P/4)$ and (9R), we find that the numerator equals a_τ; hence, we end up with

$$|\sin(\omega)| \leq \|\mathcal{A} - \cos(\omega)\|\tau_M \leq (\|\mathcal{A}\| + 1)\tau_M. \quad \text{(A.3)}$$

Equation (3) expresses the fact that if we know that the norm $\|\mathcal{A}\|$ does not exceed a certain fixed value, then the frequency ω tends to 0 if the traveling rate τ_M does so. For the extreme case of a pure standing feature ($\tau_M = 0$) we see that there cannot be any oscillation.

Now let us suppose that we work in an n-dimensional EOF space. If we use, for a vector $x = (x_1 \cdots x_n)$, the norm $|x| = \sum_i |x_i|$, the induced matrix norm is given by $\|\mathcal{A}\| = \max_j \sum_i |a_{ij}|$, with a_{ij} being the entries of $\mathcal{A}$. By the Cauchy–Schwarz inequality we find for the entries of the lag 1 covariance matrix

$$\langle q_i(t+1)q_j(t)\rangle \leq \sigma_i\sigma_j, \qquad (A.4)$$

where σ_i denotes the standard deviation for the ith EOF component. In the EOF space the lag 0 covariance matrix is diagonal, and it is easy to compute its inverse. Thus, denoting the smallest σ_i by $\sigma_{\min}$ and the average deviation $\sum_i \sigma_i/n$ by $\bar{\sigma}$, we find that the norm $\|\mathcal{A}\|$ is bounded by $\bar{\sigma}/\sigma_{\min}n$. Inserting this value into (3) we conclude:

$$\sin(\omega) \leq \left(\frac{\bar{\sigma}n}{\sigma_{\min}} + 1\right)\tau_M. \qquad (A.5)$$

REFERENCES

Barnett, T., 1983: Interaction of the monsoon and Pacific trade wind system at interannual time scales I. *Mon. Wea. Rev.*, **111**, 756–73.

Blumenthal, B., 1991: Predictability of a coupled ocean–atmosphere model. *J. Climate*, **4**, 767–784.

Brillinger, D., 1975: *Time Series. Data Analysis and Theory.* Holt, Rinehart and Winston, 540 pp.

Hasselmann, K., 1988: PIPs and POPs. The reduction of complex dynamical systems using Principal Interaction and Oscillation Patterns. *J. Geophys. Res.*, **93**, 11 015–11 021.

Latif, M., A. Sterl, E. Meier-Reimer, and M. Junge, 1993: Structure and predictability of the El Niño/Southern Oscillation phenomenon in a coupled ocean–atmosphere general circulation model. *J. Climate*, **6**, 700–708.

McCreary, J., and D. Anderson, 1991: An overview of coupled ocean–atmospheric models of El Niño and the Southern Oscillation. *J. Geophys. Res.*, **96**, 3125–3150.

Madden, R., P. and Julian, 1972: Description of global-scale circulation cells in the tropics with 40–50 day period. *J. Atmos. Sci.*, **24**, 1109–1123.

North, G., 1984: Empirical orthogonal functions and normal modes. *J. Atmos. Sci.*, **41**, 879–887.

Reynolds, R., 1988: A real-time global sea surface temperature analysis. *J. Climate*, **1**, 75–86.

Storch, H.v., T. Bruns, I. Fischer-Bruns, and K. Hasselmann, 1988: Principal oscillation patterns analysis of the 30–60-day oscillation in general circulation model equatorial troposphere. *J. Geophys. Res.*, **93**(D9), 11 022–11 036.

——, U. Weese, and J. Xu, 1990: Simultaneous analysis of space–time variability: Principal oscillation patterns and principal interaction patterns with applications to the Southern Oscillation. *Z. Meteorol.*, **40**(2), 99–103.

Wallace, J., and R. Dickinson, 1972: Empirical orthogonal representation of time series in the frequency domain I. *J. Appl. Meteor.*, **11**, 6, 887–892.

Wright, P., 1985: The Southern Oscillation. An ocean–atmosphere feedback system? *Bull. Amer. Meteor. Soc.*, **66**, 398–412.

Xu, J., and H.v., Storch, 1990: Predicting the state of the Southern Oscillation using principal oscillation pattern analysis. *J. Climate*, **3**, 1316–1329.